



HAL
open science

Arrival-angle effects on two-receiver measurements of phase velocity

Fabrizio Magrini, Giovanni Diaferia, Lapo Boschi, Fabio Cammarano

► **To cite this version:**

Fabrizio Magrini, Giovanni Diaferia, Lapo Boschi, Fabio Cammarano. Arrival-angle effects on two-receiver measurements of phase velocity. *Geophysical Journal International*, 2020, 220, pp.1838-1844. 10.1093/gji/ggz560 . insu-03691317

HAL Id: insu-03691317

<https://insu.hal.science/insu-03691317>

Submitted on 6 Sep 2022

HAL is a multi-disciplinary open access archive for the deposit and dissemination of scientific research documents, whether they are published or not. The documents may come from teaching and research institutions in France or abroad, or from public or private research centers.

L'archive ouverte pluridisciplinaire **HAL**, est destinée au dépôt et à la diffusion de documents scientifiques de niveau recherche, publiés ou non, émanant des établissements d'enseignement et de recherche français ou étrangers, des laboratoires publics ou privés.

Arrival-angle effects on two-receiver measurements of phase velocity

Fabrizio Magrini¹, Giovanni Diaferia¹, Lapo Boschi^{2,3,4} and Fabio Cammarano¹

¹Department of Sciences, Università degli Studi Roma Tre, Italy. E-mail: fabrizio.magrini@uniroma3.it

²Dipartimento di Geoscienze, Università degli Studi di Padova, Italy

³Sorbonne Université, CNRS, INSU, Institut des Sciences de la Terre de Paris, IStEP UMR 7193, F-75005 Paris, France

⁴Istituto Nazionale di Geofisica e Vulcanologia, Sezione di Bologna, Bologna, Italy

Accepted 2019 December 6. Received 2019 December 6; in original form 2019 September 30

SUMMARY

We compile a data set of Rayleigh-wave phase velocities between pairs of stations, based on teleseismic events located on the same great circle as the two stations. We validate our observations against dispersion estimates based on ambient-noise cross correlations at the same station pairs. Discrepancies between the results of the two methods can in principle be explained by deviations in the wave propagation path between earthquake and receivers, due to lateral heterogeneity in the Earth's structure, but the latter effect has, so far, not been precisely quantified nor corrected for. We implement an algorithm to measure the arrival angle of earthquake-generated surface waves and correct the dispersion measurements accordingly. Application to a data set from the Central-Western Mediterranean shows that the arrival-angle correction almost entirely accounts for the discrepancy in question, decreasing significantly the velocity bias for a wide range of periods.

Key words: Seismic interferometry; Surface waves and free oscillations; Theoretical seismology.

1 INTRODUCTION

Surface wave phase velocities from teleseismic events and ambient noise interferometry (AN, e.g. Shapiro *et al.* 2005; Boschi & Weemstra 2015) have proven fundamental in imaging the Earth at different scales. Whereas seismic noise is dominated by relatively high frequencies and therefore provides information on shallow structures, data from teleseismic earthquakes allow investigating deeper regions of the Earth (e.g. Zhou *et al.* 2012). The two-station method (e.g. Meier *et al.* 2004; Soomro *et al.* 2016) has been successfully used in regional studies for retrieving earthquake-based (EQ) measurements (e.g. Darbyshire & Lebedev 2009; Kästle *et al.* 2018). This method provides interstation phase velocities of surface waves and allows a direct comparison of AN and EQ measurements.

A number of studies have reported a discrepancy between AN and EQ phase velocities, with the latter being, on average, ~ 1 per cent higher than the former for a wide range of periods (Yao *et al.* 2006; Kästle *et al.* 2016). A ~ 1 per cent error in observed phase-velocity values would result in a similar error on estimates of shear velocity, based on the same data, at crustal and upper mantle depths (Boschi & Ekström 2002); these, in turn, could be interpreted in terms of significant thermal and/or compositional anomalies (e.g. Cammarano *et al.* 2003; Diaferia & Cammarano 2017). The origin of the systematic AN-EQ discrepancy is not yet understood; differences in AN versus EQ sensitivity kernels (Fichtner *et al.* 2016), overtone contamination (Soomro *et al.* 2016) and off-path propagation of the earthquake between epicentre and stations (Kästle

et al. 2016) have all been invoked as possible explanations. Seismic ambient noise is only approximately diffuse (Boschi & Weemstra 2015, and references therein), but inhomogeneity in noise source distribution would not explain the discrepancy in question, as it would result in AN velocity estimates systematically higher than EQ ones.

In this study, we explore in some depth the latter hypothesis, that is that deviations of the teleseismic Rayleigh-wave propagation paths from the first-order prediction (the great circles connecting source and receivers) might result in a significant *overestimate* of EQ-estimated phase velocity. We summarize the theory and our implementation in Sections 2 through 4, and present an application to seismograms from the Central-Western Mediterranean area in Section 5. The discrepancy between AN and EQ is discussed in light of the differences between phase velocities obtained before and after correcting for arrival azimuth.

2 THEORY

Assuming that phase-velocity dispersion can be retrieved by decomposition of the wave train into a sum of monochromatic, or plane waves, (e.g. Ekström *et al.* 1997), a fundamental-mode surface wave can be written (e.g. Aki & Richards 1980)

$$u(x, t) = \frac{1}{2\pi} \int_{-\infty}^{+\infty} A(\omega, x) e^{-i\phi(\omega)} e^{i\omega t} d\omega, \quad (1)$$

with

$$A(\omega, x) = I(\omega) S(\omega) R(\omega, x), \quad (2)$$

and

$$\phi(\omega) = \frac{\omega x}{c(\omega)}. \quad (3)$$

In the above equations, x , ω , t and i denote epicentral distance, angular frequency, time, and the imaginary unit, respectively; $c(\omega)$ is the phase velocity, $I(\omega)$ the instrument response (complex), $S(\omega)$ the source spectrum (complex) and $R(\omega, x)$ the path response (real), which also accounts for attenuation. Neglect of higher modes relies upon the assumption that the seismic source be distant enough from the receiver to allow their separation from the fundamental mode (Russel 1987). In the frequency domain, expression (1) can be written

$$U(\omega) = I(\omega) S(\omega) R(\omega) e^{-i\phi(\omega)}. \quad (4)$$

Let us consider a teleseismic event recorded at two seismic stations, and assume receivers and source lie approximately on the same great-circle path. The seismogram recorded at the most distant station can be expressed as the convolution of the other seismogram with a transfer function $F(\omega)$ (e.g. Darbyshire *et al.* 2004). In the frequency domain,

$$U_2(\omega) = U_1(\omega) F(\omega), \quad (5)$$

where the subscripts 1 and 2 refer to the stations. Dividing both sides by U_1 and substituting (2) into the resulting equation,

$$\frac{R_2(\omega)}{R_1(\omega)} e^{-i[\phi_2(\omega) - \phi_1(\omega)]} = F(\omega). \quad (6)$$

It is understood that the function $S(\omega)$ is the same for all stations. As for $I(\omega)$, we assume that all stations are equipped with equal sensors, in phase with each other; if that is not the case, instrument responses must be deconvolved prior to this analysis. Based on eq. (3) and provided that the source and both stations lie, to a good approximation, on the same great-circle path,

$$\phi_2(\omega) - \phi_1(\omega) = \frac{\omega(x_2 - x_1)}{c_{12}(\omega)}, \quad (7)$$

where c_{12} is the average phase velocity between stations 1 and 2.

Eqs (6) and (7) show that the phase of the transfer function is equal to the interstation average propagation phase. The phase delay $\phi_2 - \phi_1$ is also obtained by cross correlating U_1 and U_2 in the frequency domain, and measuring the phase of the resulting complex function, that is

$$U_2^*(\omega)U_1(\omega) = |U_1(\omega)||U_2(\omega)| e^{i[\phi_2(\omega) - \phi_1(\omega)]}, \quad (8)$$

where $*$ denotes complex conjugation.

3 PHASE-VELOCITY MEASUREMENTS

We implement two different approaches for retrieving interstation phase-velocity measurements: frequency-domain and time-domain. Both approaches allow to measure Rayleigh- and Love-wave phase velocities, using the vertical (or radial) and the transverse components of the recorded seismograms, respectively.

3.1 Frequency-domain

Given two recordings covering the same time window, for each investigated period the data are narrow bandpass filtered in the

frequency domain about this period, and the fundamental mode is isolated by tapering the time-series in the time domain about the arrival time predicted by the reference model (e.g. Herrin & Goforth 1977; Goforth & Herrin 1979). The effects of random noise and multipathing are reduced by further windowing the seismograms thus obtained (e.g. Ekström *et al.* 1997). We accomplish this in two ways: (I) by tapering in time domain the two filtered seismograms about the maximum of their envelope, before multiplying them in the frequency domain to finally measure the phase delay via eq. (8). Alternatively, (II) by cross-correlating the data in the time domain, to then taper the cross-correlation function about its maximum (as in Meier *et al.* 2004), and finally Fourier-transform the cross-correlation and measure dispersion in the frequency domain, again via eq. (8). In what follows we refer to these two methods as ‘t-tapering’ and ‘x-tapering’, respectively.

It should be noted that the phase delay thus calculated is affected by an intrinsic ambiguity in phase in multiples of 2π (e.g. Herrin & Goforth 1977; Ekström *et al.* 1997; Soomro *et al.* 2016):

$$c_{12}(\omega) = \frac{\omega(x_2 - x_1)}{\phi_2(\omega) - \phi_1(\omega) + 2n\pi}, \quad (9)$$

where n is integer. This ambiguity is particularly conspicuous at short periods and large interstation distances, where multiple phase-velocity solutions exist with absolute values similar to the reference ones (Section 3.3).

3.2 Time-domain

Given a teleseismic surface wave recorded at two receivers, the maximum of the cross-correlation of the bandpass filtered seismograms coincides with the traveltime of the wave train, at the frequency of interest, between one station and the other. After isolating the fundamental mode and removing disturbing factors like noise and multipathing effects, one can measure the interstation phase velocity directly in the time domain. This approach does not suffer from the above-mentioned frequency-domain ambiguities in propagation phase.

3.3 Removal of ambiguities and noisy measurements

Our procedure for identifying a unique dispersion curve for a source–stations triplet consists of three steps. (I) Selection of the most plausible phase velocities in presence of multiple measurements at a given frequency: this iterative procedure starts at the longest recorded period since phase ambiguity tends to disappear with growing period, and the phase velocity can be estimated simply by picking the value closest to a reference model. Similarly to Ekström *et al.* (1997), the phase velocity at the next, shorter period is then selected on the basis of a smoothness criterion, and the procedure is iterated for decreasing periods. Estimates that fall outside a range of tolerance are rejected. (II) Removal of noisy measurements among the velocities thus selected: whenever jumps or decreasing velocities with increasing periods occur in the dispersion curves, these are removed on the basis of velocity-gradient thresholds. In practice, at each period where a measurement is made, the range of tolerance for the following, shorter-period observation is established by linear extrapolation, based on the derivative of the reference model velocity with respect to period. If a measurement falls outside this range it is rejected. This is justified by the fact that the averaging properties of the surface-wave dispersion with depth make such segments unrealistic. (III) Dispersion curves that

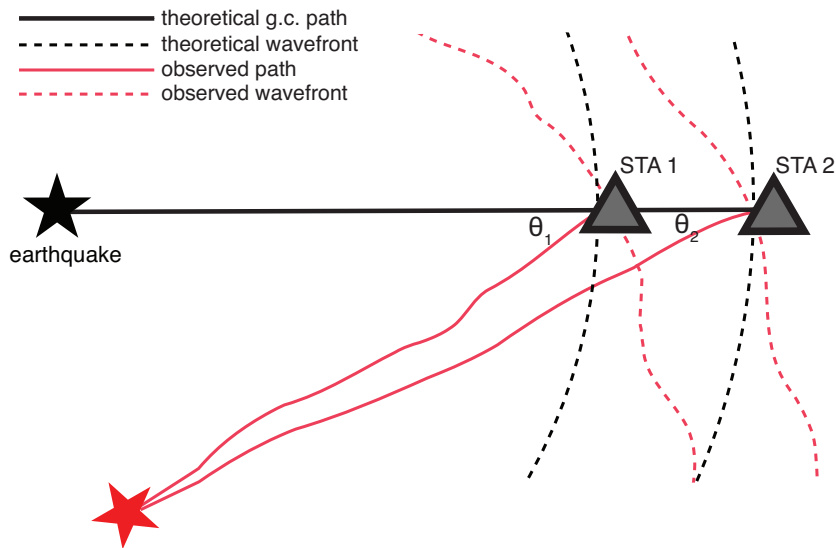


Figure 1. Sketch representing a theoretical (black curve) and observed (red curve) propagation paths of a surface wave in case of wavefront distortion due to structural heterogeneities, and/or earthquake misalignment with respect to the receivers. θ_1 and θ_2 denote the apparent arrival angles of the surface wave at stations 1 and 2, respectively.

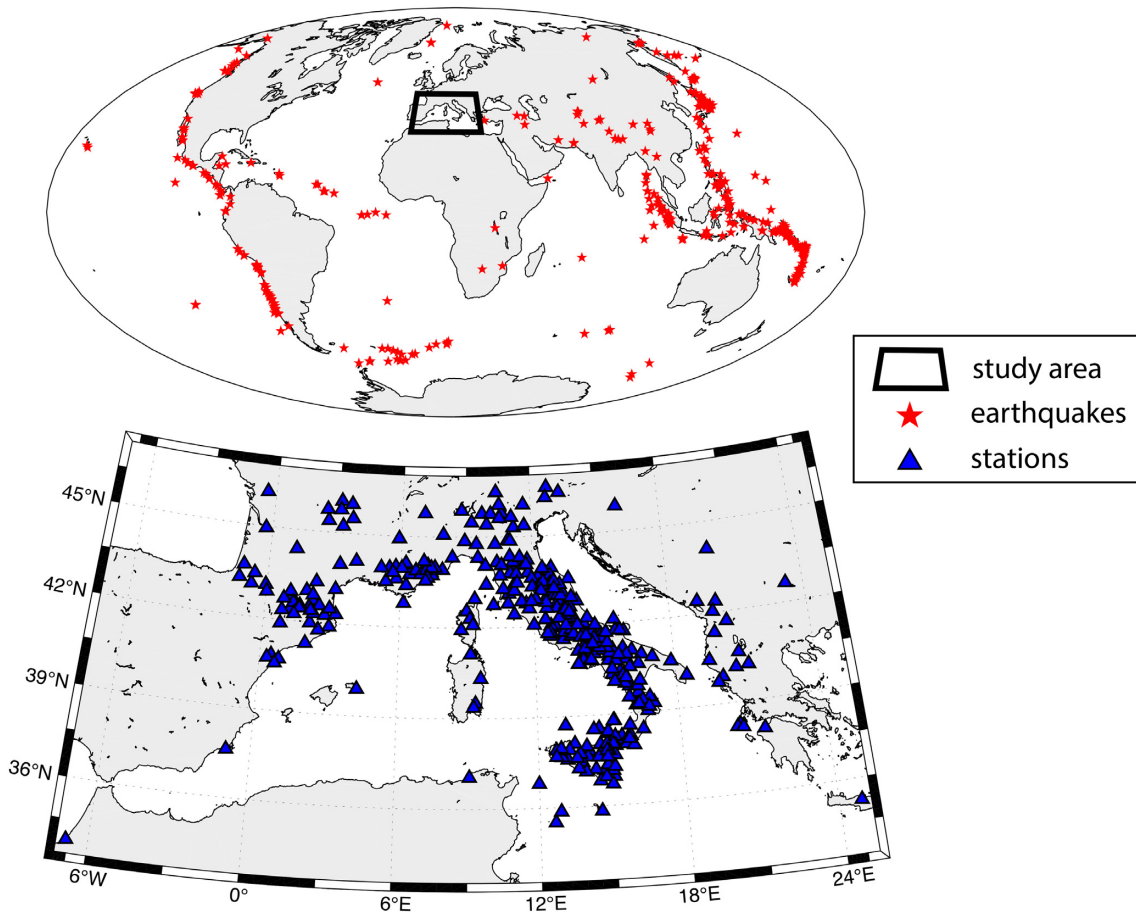


Figure 2. Earthquakes' epicentres exploited for this study (top panel) and geographic locations of the receivers within the investigated area (bottom panel). The public stations belong to the AC, CA, CR, FR, GE, HL, IV, MN, RD, TT and WM networks.

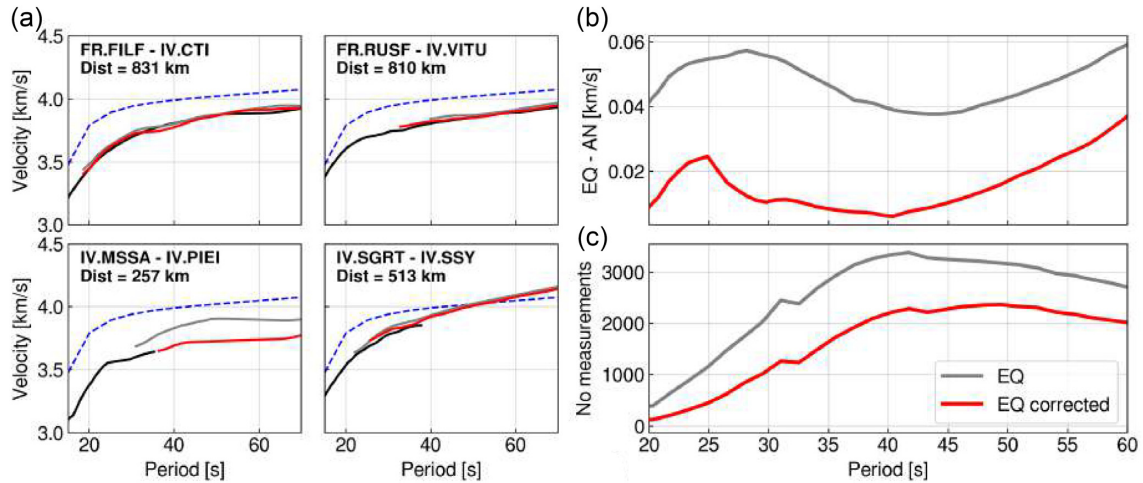


Figure 3. (a) Dispersion curves obtained for four selected station pairs following the procedure described in Section 5.1 (station acronyms and interstation distances as indicated), (b) differences between the dispersion curves obtained from the AN and EQ methods, averaged over all pairs and (c) number of measurements used for the comparison as function of period. The black, grey and red curves show the results of the AN method and the EQ method without and with arrival-angle correction, respectively. The dashed blue lines show reference velocity values (PREM, Dziewonski & Anderson 1981).

cover a very short period-range (shorter than a preliminarily selected threshold) are rejected (e.g. Soomro *et al.* 2016).

We seek values of phase velocity within ± 15 per cent of theoretical values obtained based on the PREM (Dziewonski & Anderson 1981) reference model. Velocity-gradient thresholds are set to -1.5 and 2 per cent of the PREM gradient at a given period. The minimum span of the period range for a dispersion measurement to be considered valid is set to 5.5 s. All parameters were selected via numerous preliminary runs of our algorithm, as illustrated in supplementary material.

4 CORRECTION FOR ARRIVAL AZIMUTHS

Earth's lateral heterogeneity results in deviations of the propagation path from the great circle connecting source and receivers (Fig. 1). This phenomenon has been widely observed at both short and long periods (see, for example, Laske 1995, and references therein) and can lead to overestimation of phase velocity. While several implementations of the *one*-station method account for this effect (e.g. Laske & Masters 1996), deviations from the great-circle paths are often neglected in the two-station one (e.g. Darbyshire *et al.* 2004). This is in agreement with the fact that EQ velocity estimates are systematically higher than AN ones. We address this issue by measuring the frequency-dependent arrival azimuths. This correction also accounts for both slight misalignments of the epicentre and stations and errors in source localization.

4.1 Search for the arrival azimuth

Because the radial and vertical components of a Rayleigh wave are phase-shifted by $\pi/2$, the Hilbert transform (e.g. Claerbout 1985) of the radial component is approximately in phase with the vertical one (e.g. Stachnik *et al.* 2012; Ensing & van Wijk 2018). We accordingly estimate Rayleigh-wave arrival angle by seeking the angle θ for which the squared difference between the vertical and Hilbert-transformed radial component is minimum, that is we minimize the

cost function

$$C(\theta) = \sum_i^n \left| \frac{z_i(t)}{|z(t)|_{\max}} - \frac{H_i\{r_\theta(t)\}}{|H\{r_\theta(t)\}|_{\max}} \right|^2, \quad (10)$$

where θ is the rotation angle, $H_i\{r_\theta(t)\}$ is the Hilbert-transformed radial component, $z(t)$ is the vertical component, and the subscript i indicates the i th time sample. This approach has been chosen on the basis of a suite of synthetic tests, whose results are illustrated and discussed in supplementary materials. In practice, for a large number of station pairs approximately aligned on the same great circle path as the epicentre, the radial component at both stations is simulated by shifting of $\pi/2$ the observed vertical component and adding random noise. Over a range of noise amplitudes and at most of the investigated periods, expression (10) showed a better accuracy and lower variance in retrieving the arrival angle (i.e. 0°) in comparison to other methods based on cross correlation (e.g. Stachnik *et al.* 2012).

4.2 Phase-velocity correction

In practice, the minimum of $C(\theta)$ is sought at each investigated period, to account for the dependency of wavefront distortion on frequency. At each period, the two arrival azimuths thus retrieved (one per station) are then averaged and used for calculating the arrival angle of the wave front with respect to the interstation great-circle path, similarly to Foster *et al.* (2013). Eq. (9) can then be rewritten

$$c_{12}(\omega) = \frac{\omega x \cos(\theta(\omega))}{\phi_2(\omega) - \phi_1(\omega) + 2n\pi}, \quad (11)$$

where x denotes the interstation distance and $\theta(\omega)$ the frequency-dependent average arrival angle.

For this study, the grid-search is carried out performing 60 rotations of 1° per station ($\pm 30^\circ$ from the theoretical arrival), rejecting those periods for which $C(\theta)$ did not reach a well-defined minimum in at least one of the two stations. As a result, the number of station pairs available for comparison is reduced by about 20 per cent.

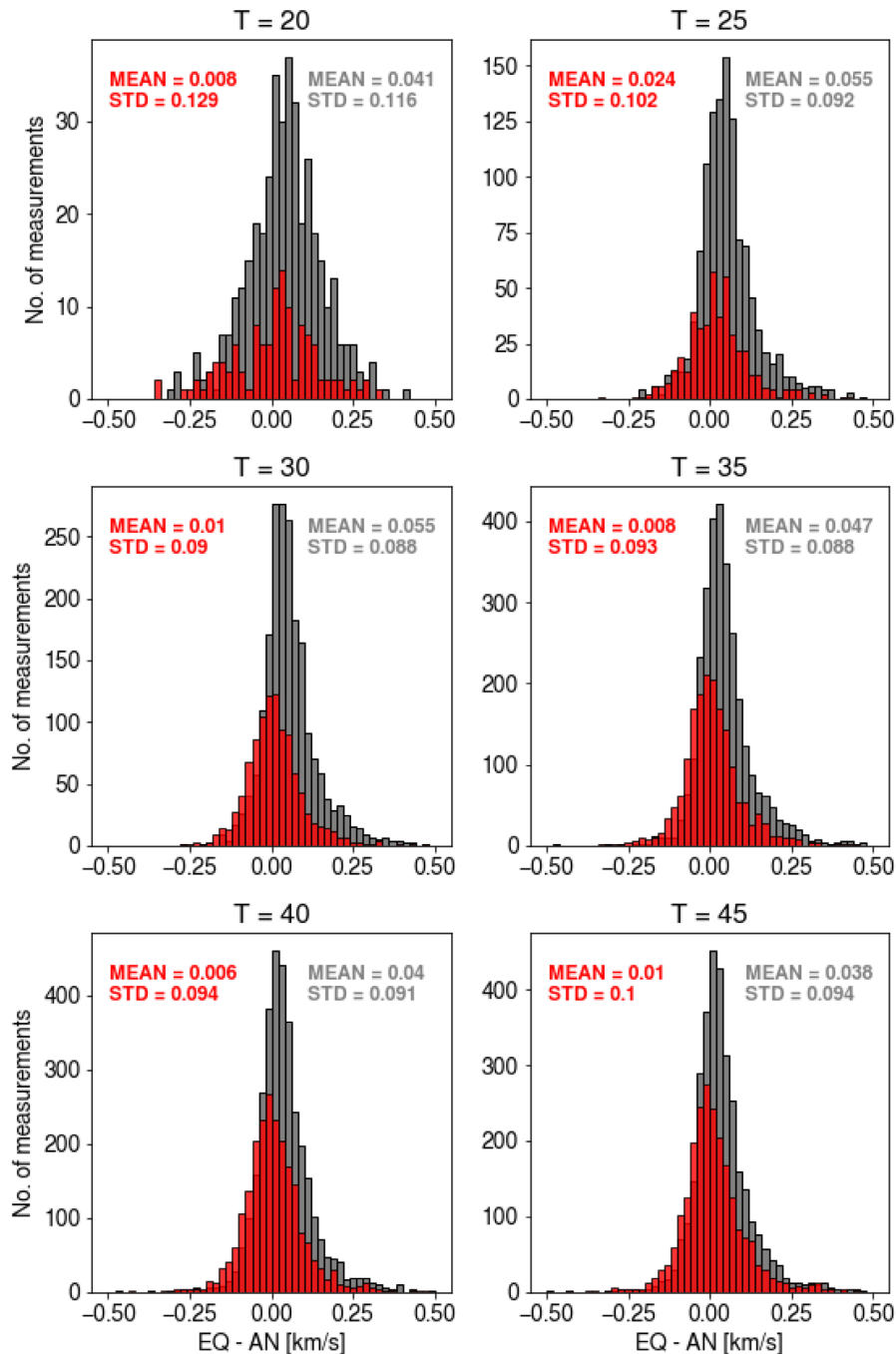


Figure 4. Histograms of phase-velocity differences between EQ and AN at the periods of 20, 25, 30, 35, 40 and 45 s. Measurements obtained with/without the correction for the arrival azimuths are indicated in red and grey, respectively.

5 APPLICATION TO CENTRAL-WESTERN MEDITERRANEAN DATA

5.1 Data set

The effects of correcting for arrival azimuth are evaluated on a data set consisting of 443 shallow teleseismic events (depths ≤ 50 km and epicentral distances between 20° and 150°) with magnitudes between 6.5 and 8.5, recorded from January 2005 to January 2019 by 361 public stations distributed across the Central-Western

Mediterranean (Fig. 2). The 3-component waveforms are demeaned, detrended and tapered (5 per cent) before deconvolving the instrument response to displacement. They are then resampled to 2 Hz and rotated to radial-transverse components using the coordinates of the epicentres. This results in 52 248 triplets of stations and sources approximately lying along the same great circle path (we set a maximum azimuthal deviation of 5°) and 16 287 station pairs to be used for comparing the dispersion curves obtained from EQ and AN.

We compiled a new data set of AN measurements based on the vertical component of continuous waveforms, by means of an automated algorithm that measures interstation phase velocities by

cross-correlation in frequency domain and stacking of noise records, as fully explained in Kästle *et al.* (2016).

For the same stations, we also compiled a new data set based on the EQ method, according to the following procedure. For each exploitable earthquake, we calculate three independent dispersion curves using both the frequency-domain (t-tapering and x-tapering) and the time-domain approaches. We have found that the three methods provide dispersion curves that differ only slightly; since there is no simple way to establish which method is most reliable, we prefer to use them all thus creating some redundancy in the data. This helps obtaining robust results, especially for station pairs that are only aligned with few events. The set of dispersion curves thus obtained for the considered station pair (three dispersion curves per event) is then cleaned from outliers [we follow the Interquartile Range rule (Tukey 1977) with outlier constant set to 0.05], and those frequencies for which less than three good measurements are available are rejected. Finally, the remaining measurements are running-averaged to obtain one smooth dispersion curve (Fig. 3a).

5.2 Results and discussion

The above procedure allowed us to retrieve $\sim 12\,000$ EQ interstation dispersion curves corrected for the arrival azimuth and $\sim 15\,000$ ones without applying the correction; the lower amount of EQ-corrected dispersion curves stems from the grid-search criteria described in Section 4.2, which result in the rejection of a greater number of measurements than EQ without correction. The discrepancy between results from AN and EQ without correction is roughly ~ 1 per cent of the AN phase velocity, similar to previous studies (e.g. Yao *et al.* 2006; Kästle *et al.* 2016, 2018), and significant, for example from the point of view of tomographic imaging and geodynamic interpretation. The correction leads to a significant improvement of the EQ-AN fit at periods of 20–50 s (Fig. 3b). The same applies to the differences between individual EQ and AN dispersion curves analysed as a function of frequency (Fig. 4). At each period the mean difference obtained after correcting is significantly closer to zero than before the correction, but the standard deviations have the same order of magnitude.

We infer that most of the previously reported discrepancy between AN and EQ can be explained by the neglect of wavefront distortion. Accounting for the arrival azimuths results in a >300 per cent decrease of the velocity bias at most of the investigated periods. By means of a Kolmogorov–Smirnov test (e.g. Press *et al.* 1992), we found that the probability for the histograms of EQ and EQ-corrected (Fig. 4) to correspond to the same statistical distribution is ~ 4 per cent at 20 s, and systematically below 1 per cent at longer periods, indicating that the improvement brought by arrival-angle correction is statistically significant.

Our arrival-angle correction appears to be particularly effective for periods of 50 s and lower, at least for the data set investigated. Above 50 s, we observe non-negligible differences between AN and EQ-corrected, with the latter being systematically faster; yet at those periods the AN signal is weaker and the AN method accordingly less reliable (e.g. Boschi & Weemstra 2015). The bias between EQ and AN is characterized by a relative maximum at periods of ~ 25 –30 s (Fig. 3.3 b), confirming earlier observations by Yao *et al.* (2006) and Kästle *et al.* (2016). This effect may be related to stronger lateral heterogeneity at relatively short periods (sensitive to shallow structures), which would result in large arrival angles and is not taken into account by our purely linear (geometric) correction.

6 CONCLUSIONS

We implemented an algorithm to improve two-station observation of earthquake-based surface wave dispersion, accounting for wavefront deviations caused by the Earth's lateral heterogeneity. The method maximizes the resemblance of the vertical component to the Hilbert-transformed radial component of the seismograms (eq. 10), and allows measuring the frequency-dependent average arrival angle of the Rayleigh wave at the receivers. One can thus retrieve the apparent interstation distance to be used for calculating the true frequency-dependent phase delay, avoiding to overestimate the phase velocity.

We applied this method to a data set from the Central-Western Mediterranean. The comparisons between ambient-noise and earthquake-based phase velocities prove that most of the systematic bias between the two methods can be ascribed to the wave train deviations from the theoretical propagation paths (great circles connecting source and receivers). The arrival-angle correction almost entirely accounts for the discrepancy in question, decreasing the velocity bias by more than ~ 300 per cent at most of the investigated periods; this confirms that the wavefront distortion effect is important and that our correction is effective.

Our method for measuring the arrival angle of the Rayleigh waves at the receivers proved to be more effective than previous attempts, albeit not error-free, as demonstrated by the synthetic tests. The observed residual bias in velocity may be related to the difficulty in measuring large arrival angles due to strong lateral heterogeneity in the Earth's structure, which would not be accounted for by our purely linear (geometric) correction. However, only further investigations may better clarify both the origin of such a residual and the role of the upper lithosphere in the wave front distortion: this will be the subject of a future study.

ACKNOWLEDGEMENTS

We are grateful to two anonymous reviewers for their insightful and constructive reviews. We thank Thomas Meier and Sebastian Lauro for their helpful comments and all the network operators providing data to the EIDA archive (<http://www.orfeus-eu.org/eida>). We thank the makers of Obspy (Beyreuther *et al.* 2010). Graphics were created with Python Matplotlib (Hunter 2007). The Grant to Department of Science, Roma Tre University (MIUR-Italy Dipartimenti di Eccellenza, ARTICOLO 1, COMMI 314-337 LEGGE 232/2016) is gratefully acknowledged.

REFERENCES

- Aki, K. & Richards, P.G., 1980, *Quantitative Seismology*, Vols I and II, University Science Books.
- Beyreuther, M., Barsch, R., Krischer, L., Megies, T., Behr, Y. & Wassermann, J., 2010. ObsPy: a Python toolbox for seismology, *Seismol. Res. Lett.*, **81**(3), 530–533.
- Boschi, L. & Ekström, G., 2002. New images of the Earth's upper mantle from measurements of surface wave phase velocity anomalies, *J. geophys. Res.*, **107**(B4), ESE–1.
- Boschi, L. & Weemstra, C., 2015. Stationary-phase integrals in the cross-correlation of ambient noise, *Rev. Geophys.*, **53**, doi:10.1002/2014RG000455.
- Cammarano, F., Goes, S., Vacher, P. & Giardini, D., 2003. Inferring upper-mantle temperatures from seismic velocities, *Phys. Earth planet. Inter.*, **138**(3–4), 197–222.
- Clairbout, J.F., 1985, *Fundamentals of Geophysical Data Processing with Applications to Petroleum Prospecting*, Blackwell Science Inc.

- Darbyshire, F.A. & Lebedev, S., 2009. Rayleigh wave phase-velocity heterogeneity and multilayered azimuthal anisotropy of the Superior Craton, Ontario, *Geophys. J. Int.*, **176**(1), 215–234.
- Darbyshire, F.A. *et al.*, 2004. A first detailed look at the Greenland lithosphere and upper mantle, using Rayleigh wave tomography, *Geophys. J. Int.*, **158**(1), 267–286.
- Diaferia, G. & Cammarano, F., 2017. Seismic signature of the continental crust: what thermodynamics says. An example from the Italian Peninsula, *Tectonics*, **36**(12), 3192–3208.
- Dziewonski, A.M. & Anderson, D.L., 1981. Preliminary reference Earth model, *Phys. Earth planet. Inter.*, **25**(4), 297–356.
- Ekström, G., Tromp, J. & Larson, E.W.F., 1997. Measurements and global models of surface wave propagation, *J. geophys. Res.*, **102**(B4), 8137–8157.
- Ensing, J.X. & van Wijk, K., 2018. Estimating the orientation of borehole seismometers from ambient seismic noise, *Bull. seism. Soc. Am.*, **109**(1), 424–432.
- Fichtner, A., Stehly, L., Ermert, L. & Boehm, C., 2016. Generalised interferometry—I. Theory for inter-station correlations, *Geophys. J. Int.*, **208**, 603–638.
- Foster, A., Ekström, G. & Nettles, M., 2013. Surface wave phase velocities of the Western United States from a two-station method, *Geophys. J. Int.*, **196**(2), 1189–1206.
- Goforth, T. & Herrin, E., 1979. Phase-matched filters: application to the study of Love waves, *Bull. seism. Soc. Am.*, **69**(1), 27–44.
- Herrin, E. & Goforth, T., 1977. Phase-matched filters: application to the study of Rayleigh waves, *Bull. seism. Soc. Am.*, **67**(5), 1259–1275.
- Hunter, J.D., 2007. Matplotlib: a 2D graphics environment, *Comput. Sci. Eng.*, **9**(3), 90–95.
- Kästle, E., Soomro, R., Weemstra, C., Boschi, L. & Meier, T., 2016. Two-receiver measurements of phase velocity: cross-validation of ambient-noise and earthquake-based observations, *Geophys. J. Int.*, **207**, 1493–1512.
- Kästle, E., El-Sharkawy, A., Boschi, L., Meier, T., Rosenberg, C.L., Bellahsen, N., Cristiano, L. & Weidle, C., 2018. Surface-wave tomography of the Alps using ambient-noise and earthquake phase-velocity measurements, *J. geophys. Res.*, **123**, doi:10.1002/2017JB014698.
- Laske, G., 1995. Global observation of off-great-circle propagation of long-period surface waves, *Geophys. J. Int.*, **123**(1), 245–259.
- Laske, G. & Masters, G., 1996. Constraints on global phase velocity maps from long-period polarization data, *J. geophys. Res.*, **101**(B7), 16 059–16 075.
- Meier, T., Dietrich, K., Stöckhert, B. & Harjes, H.-P., 2004. One-dimensional models of shear wave velocity for the eastern Mediterranean obtained from the inversion of Rayleigh wave phase velocities and tectonic implications, *Geophys. J. Int.*, **156**(1), 45–58.
- Press, W., Teukolsky, S., Vetterling, W. & Flannery, B., 1992. *Numerical Recipes in Fortran 77*, Cambridge Univ. Press.
- Russel, D., 1987. Multi-channel processing of dispersed surface-waves, *PhD dissertation*, Saint Louis University.
- Shapiro, N.M., Campillo, M., Stehly, L. & Ritzwoller, M.H., 2005. High-resolution surface-wave tomography from ambient seismic noise, *Science*, **307**(5715), 1615–1618.
- Soomro, R., Weidle, C., Cristiano, L., Lebedev, S. & Meier, T., 2016. Phase velocities of Rayleigh and Love waves in central and northern Europe from automated, broad-band, interstation measurements, *Geophys. J. Int.*, **204**(1), 517–534.
- Stachnik, J., Sheehan, A.F., Zietlow, D., Yang, Z., Collins, J. & Ferris, A., 2012. Determination of New Zealand ocean bottom seismometer orientation via Rayleigh-wave polarization, *Seismol. Res. Lett.*, **83**(4), 704–713.
- Tukey, J., 1977. *Exploratory Data Analysis*, Addison-Wesley.
- Yao, H., van Der Hilst, R.D. & De Hoop, M.V., 2006. Surface-wave array tomography in SE Tibet from ambient seismic noise and two-station analysis—I. Phase velocity maps, *Geophys. J. Int.*, **166**(2), 732–744.
- Zhou, L., Xie, J., Shen, W., Zheng, Y., Yang, Y., Shi, H. & Ritzwoller, M.H., 2012. The structure of the crust and uppermost mantle beneath South China from ambient noise and earthquake tomography, *Geophys. J. Int.*, **189**(3), 1565–1583.

SUPPORTING INFORMATION

Supplementary data are available at [GJI](https://doi.org/10.1093/gji/ggk000) online.

Figure S1. Span of the period range covered by (a) EQ and (b) EQ-corrected dispersion curves used in the comparison with AN. The smaller number of measurements of EQ-corrected dispersion curves can be ascribed to the further selection of phase velocities connected to the research for the arrival angle.

Figure S2. Histograms of the arrival angles measured in the synthetic tests at different periods. At each periods, we show the histograms obtained by minimizing the cost function defined as expression (10) of our manuscript (green) and by maximizing expression (1) (blue). For each period and cost function, the mean (μ) and the standard deviation (σ) of the Gaussian (red) fitted to the histogram is indicated. Noise level for simulating the radial components used in the synthetic test shown here has been set to half of the maximum amplitude of the vertical component.

Please note: Oxford University Press is not responsible for the content or functionality of any supporting materials supplied by the authors. Any queries (other than missing material) should be directed to the corresponding author for the paper.